



OPEN

## Exploring the nanomechanical concepts of development through recent updates in magnetically guided system

Noor Saeed Khan<sup>1,2,4</sup>✉, Auwalu Hamisu Usman<sup>1,5</sup>, Attapol Kaewkhao<sup>6</sup>✉, Poom Kumam<sup>1,2,3</sup>✉, Phatiphat Thounthong<sup>7</sup> & Usa Wannasingha Humphries<sup>1</sup>

This article outlines an analytical analysis of unsteady mixed bioconvection buoyancy-driven nanofluid thermodynamics and gyrotactic microorganisms motion in the stagnation domain of the impulsively rotating sphere with convective boundary conditions. To make the equations physically realistic, zero mass transfer boundary conditions have been used. The Brownian motion and thermophoresis effects are incorporated in the nanofluid model. Magnetic dipole effect has been implemented. A system of partial differential equations is used to represent thermodynamics and gyrotactic microorganisms motion, which is then transformed into dimensionless ordinary differential equations. The solution methodology is involved by homotopy analysis method. The results obtained are based on the effect of dimensionless parameters on the velocity, temperature, nanoparticles concentration and density of the motile microorganisms profiles. The primary velocity increases as the mixed convection and viscoelastic parameters are increased while it decreases as the buoyancy ratio, ferro-hydrodynamic interaction and rotation parameters are increased. The secondary velocity decreases as viscoelastic parameter increases while it increases as the rotation parameter increases. Temperature is reduced as the Prandtl number and thermophoresis parameter are increased. The nanoparticles concentration is increased as the Brownian motion parameter increases. The motile density of gyrotactic microorganisms increases as the bioconvection Rayleigh number, rotation parameter and thermal Biot number are increased.

In the presence of an external magnetic field, ferrofluids (a portmanteau of liquid and ferromagnetic particles) are magnetized liquid. These fluids are colloidal liquids made up of nanoscale ferrimagnetic or ferromagnetic particles that are suspended inside a fluid transport mechanism (usually a water or organic solvent). Brownian motion causes particle suspension, but these particles do not settle under normal conditions. Furthermore, each ferromagnetic particle is coated with a surfactant to prevent clumping. Magnetic attraction of nanoscale ferromagnetic particles is weak when the van der Waals force of the surfactant is strong enough to prevent agglomeration or magnetic clumping. Ferromagnetic fluids have a wide range of applications like friction-reducing agent, angular momentum change agent, heat transfer agent, and other applications including electronic devices, analytical instruments, and medicine<sup>1-3</sup>. Due to these numerous applications, many scientists and researchers

<sup>1</sup>KMUTTFixed Point Research Laboratory, Room SCL 802 Fixed Point Laboratory, Science Laboratory Building, Department of Mathematics, Faculty of Science, King Mongkut's University of Technology Thonburi (KMUTT), Bangkok 10140, Thailand. <sup>2</sup>Center of Excellence in Theoretical and Computational Science (TaCS-CoE), Science Laboratory Building, Faculty of Science, King Mongkut's University of Technology Thonburi (KMUTT), 126 Pracha-Uthit Road, Bang Mod, Thrung Khru, Bangkok 10140, Thailand. <sup>3</sup>Department of Medical Research, China Medical University Hospital, China Medical University, Taichung 40402, Taiwan. <sup>4</sup>Division of Science and Technology, Department of Mathematics, University of Education Lahore, Lahore 54770, Pakistan. <sup>5</sup>Department of Mathematical Sciences, Faculty of Physical Sciences, Bayero University Kano, Kano, Nigeria. <sup>6</sup>Data Science Research Center, Department of Mathematics, Faculty of Science, Chiang Mai University, Chiang Mai 50200, Thailand. <sup>7</sup>Department of Teacher Training in Electrical Engineering, Renewable Energy Research Centre, Faculty of Technical Education, King Mongkut's University of Technology North Bangkok, 1518 Pracharat 1 Road, Bangsue, Bangkok 10800, Thailand. ✉email: noorsaedkhankhattak@gmail.com; attapol.k@cmu.ac.th; poom.kum@kmutt.ac.th

have accelerated the study of ferrofluid. Andersson and Vanes<sup>4</sup> investigated the effect of a magnetic dipole on ferrofluid. Zeeshan et al.<sup>5</sup> reported the mixed convection flow and heat transfer in ferromagnetic fluid over a stretching sheet with partial slip effects. Hayat et al.<sup>6</sup> investigated the effects of thermal radiation and magnetic dipole on the flow of ferromagnetic Williamson liquid past a stretched surface. Some MHD studies can be read from the references<sup>7–17</sup>.

Rotating flows and heat transfer levels over stationary spinning bodies with a revolution in forced flow are important in a wide range of engineering applications like missile re-entry, projectile motion, fiber coating, and rotating machine design. Many researchers have already studied its axis of revolution parallel to the free flow velocity to solve problems of heat transfer and fluid flow on a rotating sphere. Here are some studies on this topic<sup>18–28</sup>. However, most recently, Mahdy<sup>29</sup> investigated the concurrent effects of MHD and varying wall temperatures on the transient mixed Casson nanofluid flow at the stagnation point of the rotating sphere. Mahdy and Hossam<sup>30</sup> reported the time-mixed convective nanofluid flow from the stagnation point area of the fast rotating sphere of Newtonian's heating with microorganisms. Some other rotating flows investigations exist in the references<sup>31–33</sup>.

In perspective of the pervasive engineering applications and industry, the study of non-Newtonian fluid flows has indeed achieved an exemplary commitment. Materials exhibiting a non-linear relationship between strain rate and stress, with variable coefficient viscosity, and belongings described in the Navier–Stokes equation, are recognized as non-Newtonian fluids. Many industrial fluid processes, like molten polymers, paper production, paints, cosmetics, clay mixtures, oil recovery, food dispensation and movement of biological fluids, exhibit non-Newtonian characteristics. Several models of non-Newtonian material have been developed. However, in general, the flow equations are often more non-linear compared to Newtonian fluid equations. For these reasons, the research area of non-Newtonian fluids brings some exciting and interesting difficulties for engineers, mathematicians, and computer scientists alike. Ibrahim<sup>34</sup> provided the numerical analysis of time-dependent flow of viscous fluid due to a stretchable rotating disk with heat and mass transfer. Ibrahim et al.<sup>35</sup> studied the numerical simulation and sensitivity analysis of a non-Newtonian fluid flow inside a square chamber exposed to a magnetic field using the FDLBM approach. Interesting recent studies on non-Newtonian fluids have been conducted by various researchers<sup>36–41</sup>. The second-grade fluid model is the kindest subtype of viscoelastic fluid that can be expected for analytical solution as in<sup>42–45</sup>.

A larger percentage of nuclear and thermal-hydraulic systems requires the heat transmissions that attempt to incorporate fluid flow. A wide range of fluids and operating conditions have been verified to enhance the heat transport process. The interaction of such fluids with the existing system can help to reduce capital costs, improve working efficiency, and the design of the system. Furthermore, the involvement of cooling in several technological processes, such as engines, laptops, computers, electrical strips, is crucial to maintain the effective thermal performance of these products. Nanofluid is the attribute of a nanometer-sized particle suspended in liquid. Nanofluid has been shown to improve the thermal conductivity of the base fluid under the influence of such suspended particles, and this concept originates from the work of Choi and Eastman<sup>46</sup>, which is then clarified by several researchers. El-Shorbagy et al.<sup>47</sup> investigated numerically the mixed convection in nanofluid flow in a trapezoidal channel with different aspect ratios in the presence of porous medium. Ali et al.<sup>48</sup> examined the navigation effect of tungsten oxide nano-powder on ethylene glycol surface tension by artificial neural network and response surface methodology. Chu et al.<sup>49</sup> studied the rheological behavior of MWCNT-TiO<sub>2</sub>/5W40 hybrid nanofluid based on experiments and RSM/ANN modeling. This leads to a number of researchers to see the huge efficient flow of nanofluids under different aspects<sup>50,51,53–57</sup>.

Bioconvection is a new type of industrial and biological fluid mechanics in which the phenomenon of it arises from macroscopic convective fluid movements due to the inclusion of upwardly swimming motile microorganisms (denser than the medium). As a result, the agglomerate of the loaded self-propelled microorganisms on the liquid upper surface occurs, where it contributes to density stratification, is unstable and results in the image of the bioconvection dust clouds. Water must be a standard fluid so that these self-propelled microorganisms are active in the base fluid<sup>58–66</sup>.

Inspired mostly by the above-mentioned references to bioconvection nanofluid flows, the purpose of this paper is to examine the behavior of transient mixed stagnation point boundary layer flow of second-grade fluid across the rashly revolving sphere consisting of nanoparticles and motile gyrotactic microorganisms under magnetic dipole effects. The impetuous movement of nanofluid, microorganisms and the impulsive rotation of the sphere lead to unsteadiness. Similarity transformation approach is used to determine the non-linear ordinary differential equations and solution through the homotopy analysis method HAM<sup>67–70</sup>.

## Problem formulation

The two-dimensional time-state, laminar incompressible, mixed convection boundary layer flow of viscous electrically conducting second grade nanofluid with swimming gyrotactic microorganisms in the stagnation domain of the rotating sphere and thermal convective boundary condition is scrutinized. Recognizing the Buongiorno nanofluid model, comprising of Brownian motion and thermophoresis effects is adopted in the present investigations. It is assumed that uniform dispersion is achieved by the lack of aggregation and accretion of nanoparticles. The sphere is revolving with a constant angular velocity  $\Omega$ . At time  $t = 0$ , the sphere is at rest and the surface temperature, concentration and motile microorganisms are  $T_\infty$ ,  $C_\infty$  and  $N_\infty$  in an ambient fluid, respectively. The flow of motile microorganisms remains constant along sphere surface and zero mass flux condition is applied at the surface. The sphere surface is warmed due to convection from a warm nanofluid at the temperature  $T_\infty$  which provides a heat transfer factor  $h_f$ , is to be strengthened or weakened to the value  $T_\infty$ , where  $T_w > T_\infty$  leads to aiding flow and  $T_w < T_\infty$  leads to reversing flow, respectively. Apart from nanofluid properties, which are chosen to be constant, density variation is based on Boussinesq approximation. Both Joule heating and viscous

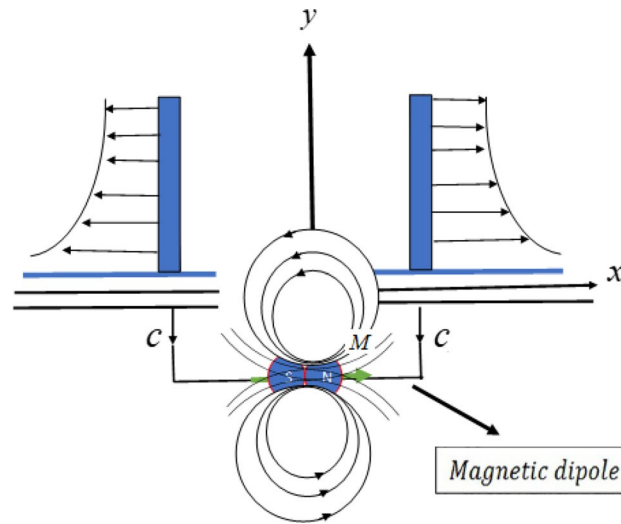


**Figure 1.** Schematic diagram of the problem.

dissipation effects have been ignored. Nanoparticles have no influence on the direction and velocity of gyrotactic microorganisms. Motile microorganisms, nanoparticles and base fluid have the same velocity.

**Magnetic dipole.** The characteristics of the magnetic field have an effect on the flow of ferrofluid due to the magnetic dipole<sup>2,4,6</sup>. Magnetic dipole effects are recognized by the magnetic scalar potential  $\Phi$  shown as in Eq. (1)

$$\Phi = \frac{\gamma}{2\pi} \frac{x}{x^2 + (y + c)^2}, \tag{1}$$

where  $\gamma$  stands for the magnetic field strength at the source. Taking  $H_x$  and  $H_y$  as the components of magnetic field as shown in Eqs. (2) and (3),

$$H_x = -\frac{\partial \Phi}{\partial x} = \frac{\gamma}{2\pi} \frac{x^2 - (y + c)^2}{[x^2 + (y + c)^2]^2}, \tag{2}$$

$$H_y = -\frac{\partial \Phi}{\partial y} = \frac{\gamma}{2\pi} \frac{2x(y + c)}{[x^2 + (y + c)^2]^2}. \tag{3}$$

Since the magnetic body strength is usually proportional to  $H_x$  and  $H_y$  gradient,  $c$  is the distance of the line currents from the leading edge, it is therefore given as in (4)

$$H = \sqrt{H_x^2 + H_y^2}. \tag{4}$$

Equation (5) can approximate the linear shape of magnetization  $M$  by temperature  $T$  as

$$M = K_1(T - T_\infty). \tag{5}$$

The value of  $K_1$  is identified as a ferromagnetic coefficient. Figure 1 shows the physical diagram of the problem about magnetic dipole.

The problem equations for second grade nanofluid with dipole effect are given as<sup>21–23,29,30,43–45</sup>

$$\frac{\partial(xu)}{\partial x} + \frac{\partial(xv)}{\partial y} = 0, \tag{6}$$

$$\begin{aligned} \frac{\partial u}{\partial t} + u \frac{\partial u}{\partial x} + w \frac{\partial u}{\partial y} - \frac{v^2}{x} &= U \frac{\partial U}{\partial x} + \nu_f \frac{\partial^2 u}{\partial y^2} \\ &+ \frac{\alpha_1}{\rho_{f_\infty}} \left[ u \frac{\partial^3 u}{\partial x \partial y^2} + v \frac{\partial^3 u}{\partial y^3} + \frac{\partial u}{\partial x} \frac{\partial^2 u}{\partial y^2} - \frac{\partial u}{\partial y} \frac{\partial^2 u}{\partial x \partial y} + \frac{\partial w}{\partial y} \frac{\partial^2 w}{\partial x \partial y} + \frac{\partial w}{\partial x} \frac{\partial^2 w}{\partial y^2} \right] + \frac{\mu_o M}{\rho_{f_\infty}} \frac{\partial H}{\partial x} \\ &+ \left[ (1 - C_\infty) \beta \rho_{f_\infty} (T - T_\infty) - (\rho_p - \rho_{f_\infty})(C - C_\infty) - (\rho_m - \rho_{f_\infty}) \gamma^* (N - N_\infty) \right] \frac{g_x}{R \rho_{f_\infty}}, \end{aligned} \tag{7}$$

$$\frac{\partial v}{\partial t} + u \frac{\partial v}{\partial x} + w \frac{\partial v}{\partial y} - \frac{uv}{x} = \frac{\mu_{f\infty}}{\rho_{f\infty}} \frac{\partial^2 v}{\partial y^2} + \frac{\alpha_1}{\rho_{f\infty}} \left[ u \frac{\partial^3 w}{\partial x \partial y^2} + v \frac{\partial^3 w}{\partial y^3} \right], \tag{8}$$

$$(c_p \rho)_{f\infty} \left( \frac{\partial T}{\partial t} + u \frac{\partial T}{\partial x} + w \frac{\partial T}{\partial y} \right) = k_f \frac{\partial^2 T}{\partial y^2} + \tau \left( D_B \frac{\partial C}{\partial y} \frac{\partial T}{\partial y} + \frac{D_T}{T_\infty} \left( \frac{\partial T}{\partial y} \right)^2 \right) + \left( u \frac{\partial H}{\partial x} + v \frac{\partial H}{\partial y} \right) \mu_o T \frac{\partial M}{\partial T}, \tag{9}$$

$$\frac{\partial C}{\partial t} + u \frac{\partial C}{\partial x} + w \frac{\partial C}{\partial y} = D_B \frac{\partial^2 C}{\partial y^2} + \frac{D_T}{T_\infty} \frac{\partial^2 T}{\partial y^2}, \tag{10}$$

$$\frac{\partial N}{\partial t} + u \frac{\partial N}{\partial x} + w \frac{\partial N}{\partial y} + \frac{bW_c}{C_\infty} \frac{\partial N}{\partial y} \left( \frac{\partial C}{\partial y} \right) = D_n \frac{\partial^2 N}{\partial y^2}. \tag{11}$$

The boundary conditions are as in<sup>29,30</sup>

$$t < 0 : u(x, y, t) = 0, v(x, y, t) = 0, w(x, y, t) = 0, T(x, y, t) = T_\infty, C(x, y, t) = C_\infty, N(x, y, t) = N_\infty, \tag{12}$$

$$t \geq 0 : u(x, 0, t) = U, v(x, 0, t) = \Omega x, w(x, 0, t) = 0, -k_f \frac{\partial T}{\partial y} = h_f(T_f - T), D_B \frac{\partial C}{\partial y} + \frac{D_T}{T_\infty} \frac{\partial T}{\partial y} = 0, N(x, 0, t) = N_w, u(x, \infty, t) \rightarrow U, v(x, \infty, t) \rightarrow 0, T(x, \infty, t) \rightarrow T_\infty, C(x, \infty, t) \rightarrow C_\infty, N(x, \infty, t) \rightarrow N_\infty, \tag{13}$$

where  $\alpha_1(>0)$  is the material parameter and  $u_w$  is the stretching velocity.

Using the following transformations as in<sup>29,30</sup>  $\zeta = \sqrt{\frac{2c_1}{v_f}} \eta^{\frac{1}{2}} y$ ,  $\eta = 1 - e^{-c_1 t}$ ,  $u(x, y, t) = c_1 x f'(\eta, \zeta)$ ,  $v(x, y, t) = \Omega g(\eta, \zeta)$ ,  $w(x, y, t) = -\sqrt{2c_1 v_f} \eta f'(\eta, \zeta)$ ,  $\theta(\zeta) = \frac{T - T_\infty}{T_w - T_\infty}$ ,  $\phi(\zeta) = \frac{C - C_\infty}{C_w - C_\infty}$ ,  $\chi(\zeta) = \frac{N - N_\infty}{N_w - N_\infty}$ , the above governing equations provide the following non-dimensional form

$$f''' + \frac{1}{2} \zeta (1 - \eta) f'' - \eta (1 + \lambda_1 g^2 - ff'^2) + A_1 (2f'f''' - f''^2) + \frac{A_2}{\sqrt{\eta}} f'''' g - \frac{2\beta\theta}{(\zeta + d)^4} + \gamma_1 \eta [\theta - Nr\phi - Rb\chi] = 0, \tag{14}$$

$$g'' + \frac{1}{4} \zeta (1 - \eta) g + \frac{1}{2} \eta (fg - f'g) - 2A_1 f'''' g = 0, \tag{15}$$

$$\theta'' + Pr \left[ \frac{1}{4} \zeta (1 - \eta) \theta' + \eta f \theta' + Nb \phi' \theta' + Nt \theta'^2 \right] + \eta \beta \lambda (\theta - \varepsilon) \frac{2\Omega g}{(\zeta + d)^3} + \eta Pr \beta \lambda (\theta - \varepsilon) \left[ \frac{2f'}{(\zeta + d)^4} + \frac{4\Omega g}{(\zeta + d)^5} \right] = 0, \tag{16}$$

$$\phi'' + Sc \left[ \frac{Nt}{Nb} \theta'' + \frac{1}{4} \zeta (1 - \eta) \phi + \eta f \phi' \right] = 0, \tag{17}$$

$$\chi'' - Pe [\chi' \phi' + (\chi + N_\delta) \phi''] + \frac{Sb}{4} \zeta (1 - \eta) \chi' + Sb \eta f \chi' = 0, \tag{18}$$

with non-dimensional boundary conditions given as

$$f(\eta, 0) = f'(\eta, 0) = 0, g(\eta, 0) - 1 = 0, \theta' = Bi(\theta - 1), Nb\phi'(\eta, 0) + Nt\theta(\eta, 0) = 0, \chi(\eta, 0) = 1, f'(\eta, \infty) \rightarrow 1, g(\eta, \infty) \rightarrow 0, \theta(\eta, \infty) \rightarrow 0, \phi(\eta, \infty) \rightarrow 0, \chi(\eta, \infty) \rightarrow 0. \tag{19}$$

Here  $c_1$  is the constant such that  $c_1 > 0$ ,  $\eta$  designates the dimensionless time parameter,  $\zeta$  indicates the converted variable,  $f'$  and  $g$  stand for the velocity components in the  $x$ - and  $y$ - directions,  $T$  means the dimensionless temperature,  $\phi$  is the dimensionless nanoparticles concentration,  $N$  is density of motile microorganisms,  $\gamma_1$  denotes the mixed convection parameter,  $Nr$  points out the buoyancy ratio,  $\beta$  is the ferrohydrodynamic interaction parameter,  $Pr$  is the Prandtl number,  $Sc$  is the traditional Schmidt number,  $Sb$  is the bioconvection Schmidt number,  $\lambda_1$  is the rotation parameter,  $\lambda$  is the heat dissipation parameter,  $\varepsilon$  is the curie temperature,  $d$  is the dimensionless distance,  $Nt$  is the thermophoresis,  $Nb$  is the Brownian motion parameter,  $N_\delta$  denotes the microorganisms concentration difference parameter,  $Rb$  gives bioconvection Rayleigh number,  $Pe$  is the bioconvection Peclet number,  $Re$  is the Reynolds number,  $A_1$  is the viscoelastic parameter,  $A_2$  is the dimensionless parameter,  $Bi$  is the thermal Biot number and  $'$  indicates the derivatives with respect to  $\zeta$ . These parameters are given in mathematical expressions by

$$\lambda_1 = \left(\frac{\Omega}{c_1}\right)^2, A_1 = \frac{c_1\alpha_1}{\mu_{f\infty}}, A_2 = \frac{\alpha_1\Omega}{\mu_{f\infty}}\sqrt{\frac{2c_1}{v_f}}, \beta = \frac{\gamma\mu_0K_1(T_\infty - T_w)\rho_{f\infty}}{2\pi\mu_{f\infty}^2}, d = \sqrt{\frac{2c_1a^2}{v_f}}, \gamma_1 = \frac{\beta T g(1 - C_\infty)(T_w - T_\infty)}{c_1^2 R},$$

$$Nr = \frac{(\rho_p - \rho_{f\infty})C_\infty}{\rho_{f\infty}\beta_T(1 - C_\infty)(T_w - T_\infty)}, Rb = \frac{(\rho_m - \rho_{f\infty})\gamma^*(N_w - N_\infty)}{\rho_{f\infty}\beta_T(1 - C_\infty)(T_w - T_\infty)}, Pr = \frac{v_f(\rho c_p)_{f\infty}}{k_f}, Nb = \frac{\tau D_B C_\infty}{v_f}, Nt = \frac{D_T(T_w - T_\infty)}{T_\infty v_f},$$

$$\lambda = \frac{c_1\mu_{f\infty}^2}{\rho_{f\infty}(T_w - T_\infty)k_T}, \varepsilon = \frac{T_\infty}{T_\infty - T_w}, Sc = \frac{v_f}{D_B}, Sb = \frac{v_f}{D_n}, Pe = \frac{bW_\infty}{D_n} \text{ and } Bi = \frac{h_f}{k_f}\left(\frac{\eta v_f}{2c_1}\right)^{\frac{1}{2}}.$$

According to the dimensionless variables, the significant designed physical quantities termed as the skin friction factor  $C_f$ , Nusselt number  $Nu$ , and the density of the motile microorganisms number  $Nn$  are given in the form

$$C_f = \frac{\tau_w}{\rho_{f\infty} U^2}, Nu = \frac{xq_r}{k_f(T_w - T_\infty)}, Nn = \frac{xq_n}{D_n(\chi_w - \chi_\infty)}, \tag{20}$$

where shear stress, surface heat and motile surface microorganisms fluxes are mathematically expressed as

$$\tau_w = \mu_{f\infty} \frac{\partial u}{\partial y} \Big|_{y=0}, q_r = -k_f \frac{\partial u}{\partial y} \Big|_{y=0}, q_n = -D_n \frac{\partial u}{\partial y} \Big|_{y=0}. \tag{21}$$

Using the similarity transformations and Eq. (21) through Eq. (20), the simplified forms are

$$Re^{\frac{1}{2}} \eta^{\frac{1}{2}} C_f = 2\sqrt{2}f''(\eta, 0),$$

$$Re^{-\frac{1}{2}} \eta^{\frac{1}{2}} Nu = -\sqrt{2}\theta'(\eta, 0), \tag{22}$$

$$Re^{-\frac{1}{2}} \eta^{\frac{1}{2}} Nn = -\sqrt{2}N'(\eta, 0),$$

where  $Re_x = \frac{cx^2}{v_f}$  is the Reynolds number.

### Solution by homotopy analysis method

For nonlinear systems of partial or ordinary differential equations, Homotopy Analysis Method (HAM) is recognized as an important alternative to the conventional numerical methods. Liao<sup>67-69</sup> proposed the Homotopy Analysis Method, which uses the basic concepts of homotopy in topology to develop an alternative and general analytical-numerical method for nonlinear problems. The validity of HAM is independent of whether or not the considered equation contains small parameter(s). As a result, HAM overcomes the limitations of perturbation methods.

Taking the initial guesses and the linear operators as

$$f_0(\zeta) = A\zeta + (1 - A)(1 - e^{-\zeta}), g_0(\zeta) = e^{-\zeta}, \theta_0(\zeta) = \frac{Bi}{1 + Bi}e^{-\zeta}, \phi_0(\zeta) = e^{-\zeta}, \chi_0(\zeta) = e^{-\zeta}. \tag{23}$$

Equation (23) satisfies the linear operators properties as given below

$$L_f(E_1 + E_2e^\zeta + E_3e^{-\zeta}) = 0, L_g(E_4e^\zeta + E_5e^{-\zeta}) = 0, L_\theta(E_6e^\zeta + E_7e^{-\zeta}) = 0,$$

$$L_\phi(E_8e^\zeta + E_9e^{-\zeta}) = 0, L_\chi(E_{10}e^\zeta + E_{11}e^{-\zeta}) = 0, \tag{24}$$

where  $E_i (i = 1, \dots, 11)$  indicates the arbitrary constants.

The corresponding zeroth order form of the problems are

$$(1 - q)L_f[f(\zeta, q) - f_0(\zeta)] = qh_f N_f[f(\zeta, q), g(\zeta, q), \theta(\zeta, q), \phi(\zeta, q), \chi(\zeta, q)],$$

$$(1 - q)L_g[g(\zeta, q) - g_0(\zeta)] = qh_g N_g[g(\zeta, q), f(\zeta, q)],$$

$$(1 - q)L_\theta[\theta(\zeta, q) - \theta_0(\zeta)] = qh_\theta N_\theta[\theta(\zeta, q), f(\zeta, q), g(\zeta, q), \phi(\zeta, q)],$$

$$(1 - q)L_\phi[\phi(\zeta, q) - \phi_0(\zeta)] = qh_\phi N_\phi[\phi(\zeta, q), \theta(\zeta, q), f(\zeta, q)],$$

$$(1 - q)L_\chi[\chi(\zeta, q) - \chi_0(\zeta)] = qh_\chi N_\chi[\chi(\zeta, q), \phi(\zeta, q), f(\zeta, q)], \tag{25}$$

with the boundary conditions

$$f(0, q) = 0, f'(0, q) = 1, f'(\infty, q) = A, g'(0, q) = 1, g(\infty, q) = 0, \theta'(0, q) = -Bi(1 - \theta(0, q)),$$

$$\theta(\infty, q) = 0, \phi'(0, q) = 1, \phi(\infty, q) = 0, \chi'(0, q) = 1, \chi(\infty, q) = 0. \tag{26}$$

The non-linear operators are given by

$$\begin{aligned} \mathbf{N}_f[f(\zeta, q), g(\zeta, q), \theta(\zeta, q), \phi(\zeta, q), \chi(\zeta, q)] &= \frac{\partial^3 f(\zeta, q)}{\partial \zeta^3} + \frac{1}{2}\zeta(1 - \eta) \frac{\partial^2 f(\zeta, q)}{\partial \zeta^2} \\ &- \eta \left( 1 + \lambda_1 g^2(\zeta, q) - f \left( \frac{\partial f(\zeta, q)}{\partial \zeta} \right)^2 \right) + A_1 \left( 2 \frac{\partial f(\zeta, q)}{\partial \zeta} \frac{\partial^3 f(\zeta, q)}{\partial \zeta^3} - \left( \frac{\partial^2 f(\zeta, q)}{\partial \zeta^2} \right)^2 \right) \\ &+ \frac{A_2}{\sqrt{\eta}} \frac{\partial^4 f(\zeta, q)}{\partial \zeta^4} g(\zeta, q) - \frac{2\beta\theta(\zeta, q)}{(\zeta + d)^4} + \gamma_1(\zeta, q)\eta[\theta(\zeta, q) - Nr\phi(\zeta, q) - Rb\chi(\zeta, q)], \end{aligned} \tag{27}$$

$$\begin{aligned} \mathbf{N}_g[f(\zeta, q), g(\zeta, q)] &= \frac{\partial^2 g(\zeta, q)}{\partial \zeta^2} + \frac{1}{4}\zeta(1 - \eta)g(\zeta, q) + \frac{1}{2}\eta(f(\zeta, q)g(\zeta, q) - \frac{\partial f(\zeta, q)}{\partial \zeta}g(\zeta, q)) \\ &- 2A_1 \frac{\partial^3 f(\zeta, q)}{\partial \zeta^3} g(\zeta, q), \end{aligned}$$

$$\begin{aligned} \mathbf{N}_\theta[\theta(\zeta, q), \phi(\zeta, q), f(\zeta, q), g(\zeta, q)] &= \frac{\partial^2 \theta(\zeta, q)}{\partial \zeta^2} \\ &+ Pr \left[ \frac{1}{4}\zeta(1 - \eta) \frac{\partial \theta(\zeta, q)}{\partial \zeta} + \eta f \theta(\zeta, q) \frac{\partial \theta(\zeta, q)}{\partial \zeta} + Nb \frac{\partial \theta(\zeta, q)}{\partial \zeta} \frac{\partial \phi(\zeta, q)}{\partial \zeta} + Nt \left( \frac{\partial \theta(\zeta, q)}{\partial \zeta} \right)^2 \right] \\ &+ \eta \beta \lambda (\theta - \varepsilon) \frac{2\Omega g(\zeta, q)}{(\zeta + d)^3} + \eta Pr \beta \lambda (\theta(\zeta, q) - \varepsilon) \left[ \frac{2}{(\zeta + d)^4} \frac{\partial f(\zeta, q)}{\partial \zeta} + \frac{4\Omega g(\zeta, q)}{(\zeta + d)^5} \right], \end{aligned} \tag{28}$$

$$\mathbf{N}_\phi[\phi(\zeta, q), \theta(\zeta, q), f(\zeta, q)] = \frac{\partial^2 \phi(\zeta, q)}{\partial \zeta^2} \tag{29}$$

$$\begin{aligned} \mathbf{N}_\chi[\phi(\zeta, q), \theta(\zeta, q), f(\zeta, q)] &= \frac{\partial^2 \phi(\zeta, q)}{\partial \zeta^2} \mathbf{N}_\chi[\chi(\zeta, q), \phi(\zeta, q), f(\zeta, q)] \\ &= \frac{\partial^2 \chi(\zeta, q)}{\partial \zeta^2} - Pe \left[ \frac{\partial \chi(\zeta, q)}{\partial \zeta} \frac{\partial \phi(\zeta, q)}{\partial \zeta} + (\chi(\zeta, q) + N_\delta) \frac{\partial^2 \phi(\zeta, q)}{\partial \zeta^2} \right] \\ &+ \frac{Sb}{4}\zeta(1 - \eta) \frac{\partial \chi(\zeta, q)}{\partial \zeta} + Sb \eta f(\zeta, q) \frac{\partial \chi(\zeta, q)}{\partial \zeta}, \end{aligned} \tag{30}$$

where  $q \in [0, 1]$  is the embedding parameter.  $\mathbf{N}_f, \mathbf{N}_g, \mathbf{N}_\theta, \mathbf{N}_\phi$  and  $\mathbf{N}_\chi$  are the nonlinear operators. The  $m$ th-order deformation problems are

$$L_f[f_m(\zeta, q) - \xi_m f_{m-1}(\zeta)] = h_f \mathcal{R}_{f,m}(\zeta), \tag{31}$$

$$L_g[g_m(\zeta, q) - \xi_m g_{m-1}(\zeta)] = h_g \mathcal{R}_{g,m}(\zeta), \tag{32}$$

$$L_\theta[\theta_m(\zeta, q) - \xi_m \theta_{m-1}(\zeta)] = h_\theta \mathcal{R}_{\theta,m}(\zeta), \tag{33}$$

$$L_\phi[\phi_m(\zeta, q) - \xi_m \phi_{m-1}(\zeta)] = h_\phi \mathcal{R}_{\phi,m}(\zeta), \tag{34}$$

$$L_\chi[\chi_m(\zeta, q) - \xi_m \chi_{m-1}(\zeta)] = h_\chi \mathcal{R}_{\chi,m}(\zeta), \tag{35}$$

with boundary conditions

$$\begin{aligned} f_m(0) = f'_m(0) = f'_m(\infty) = 0, \\ g'_m(0) = g_m(0) = g_m(\infty) = 0, \\ \theta'_m(0) - B_{i1}\theta_m(0) = \theta_m(\infty) = 0, \\ \phi'_m(0) = \phi_m(0) = \phi_m(\infty) = 0, \\ \chi'_m(0) = \chi_m(0) = \chi_m(\infty) = 0, \end{aligned} \tag{36}$$

where

$$\xi_m = \begin{cases} 0, & \text{if } m \leq 1 \\ 1, & \text{if } m > 1. \end{cases} \tag{37}$$

And

Order of approximation	$f''(0)^{28}$	$f''(0)$ (Present)	$g'(0)^{28}$	$g'(0)$ (Present)
1	1.59936137	1.59936125	0.20487518	0.20487515
2	1.59936085	1.59936081	0.204875662	0.204875661
3	1.59936095	1.59936095	0.204875662	0.204875662
15	1.59936095	1.59936095	0.204875662	0.204875662

**Table 1.** Comparison of the current work.

$$\begin{aligned} \mathcal{R}_f^m(\zeta) = & f_{m-1}''' + \frac{1}{2}\zeta(1-\eta)f_{m-1}'' - \eta \left( 1 + \lambda_1 g_{m-1}^2 - \sum_{r=0}^{m-1} \left( \sum_{k=0}^r f_{m-1-r} f_{r-k}' \right) f_k' \right) \\ & + A_1 \left( 2 \sum_{r=0}^{m-1} f_{m-1-r} f_r''' - \sum_{r=0}^{m-1} f_{m-1-r} f_r'' \right) + \frac{A_2}{\sqrt{\eta}} \sum_{r=0}^{m-1} g_{m-1-r} f_r''' - \frac{2\beta\theta_{m-1}}{(\zeta+d)^4} \\ & + \gamma_1 \eta [\theta_{m-1} - Nr\phi_{m-1} - Rb\chi_{m-1}] = 0, \end{aligned} \tag{38}$$

$$\begin{aligned} \mathcal{R}_g^m(\zeta) = & g_{m-1}'' + \frac{1}{4}\zeta(1-\eta)g_{m-1} + \frac{1}{2}\eta \left( \sum_{r=0}^{m-1} f_{m-1-r} g_r \right) - \sum_{r=0}^{m-1} (f_{m-1-r} g_r) \\ & - 2A_1 \sum_{r=0}^{m-1} f_{m-1-r} g_r, \end{aligned} \tag{39}$$

$$\begin{aligned} \mathcal{R}_\theta^m(\zeta) = & \theta_{m-1}'' + Pr \left[ \frac{1}{4}\zeta(1-\eta)\theta_{m-1}' + \eta \sum_{r=0}^{m-1} f_{m-1-r} \theta_r' + Nb \sum_{r=0}^{m-1} \phi_{m-1-r} \theta_r' + Nt \sum_{r=0}^{m-1} \theta_{m-1-r} \theta_r' \right] \\ & + \eta\beta\lambda \frac{2\Omega \sum_{r=0}^{m-1} g_{m-1-r} \theta_r}{(\zeta+d)^3} - \eta\beta\lambda \frac{2\varepsilon\Omega g_{m-1}}{(\zeta+d)^3} + \eta Pr\beta\lambda \left[ \frac{2 \sum_{r=0}^{m-1} f_{m-1-r} \theta_r}{(\zeta+d)^4} + \frac{4\Omega \sum_{r=0}^{m-1} g_{m-1-r} \theta_r}{(\zeta+d)^5} \right] \\ & - \eta Pr\beta\lambda\varepsilon \left[ \frac{2f_{m-1}'}{(\zeta+d)^4} + \frac{4\Omega g_{m-1}}{(\zeta+d)^5} \right], \end{aligned} \tag{40}$$

$$\mathcal{R}_\phi^m(\zeta) = \phi_{m-1}'' + Sc \left[ \frac{Nt}{Nb} \theta_{m-1}'' + \frac{1}{4}\zeta(1-\eta)\phi_{m-1} + \eta \sum_{r=0}^{m-1} f_{m-1-r} \phi_r' \right], \tag{41}$$

$$\begin{aligned} \mathcal{R}_\chi^m(\zeta) = & \chi_{m-1}'' + Pe \left[ \sum_{r=0}^{m-1} \phi_{m-1-r} \chi_r' + \sum_{r=0}^{m-1} \phi_{m-1-r}'' \chi_r + N\delta \phi_{m-1}'' \right] + \frac{Sb}{4}\zeta(1-\eta)\chi_{m-1}' \\ & + Sb\eta \sum_{r=0}^{m-1} f_{m-1-r} \chi_r'. \end{aligned} \tag{42}$$

The general solution is given by

$$f_m(\zeta) = f_m^*(\zeta) + E_1 + E_2 e^\zeta + E_3 e^{-\zeta}, \tag{44}$$

$$g_m(\zeta) = g_m^*(\zeta) + E_4 e^\zeta + E_5 e^{-\zeta}, \tag{45}$$

$$\theta_m(\zeta) = \theta_m^*(\zeta) + E_6 e^\zeta + E_7 e^{-\zeta}, \tag{46}$$

$$\phi_m(\zeta) = \phi_m^*(\zeta) + E_8 e^\zeta + E_9 e^{-\zeta}, \tag{47}$$

$$\chi_m(\zeta) = \chi_m^*(\zeta) + E_{10} e^\zeta + E_{11} e^{-\zeta}, \tag{48}$$

where  $f_m^*(\zeta)$ ,  $(g_m^*(\zeta), \theta_m^*(\zeta), \phi_m^*(\zeta)$  and  $\chi_m^*(\zeta)$  are the special solutions.

### Results and discussion

Solution authentication has an important role in the evaluations of the problems. Therefore, the present solution is compared with the published work. Order of approximation of the present work in Table 1 is given which presents the close agreement with the published paper results<sup>28</sup>.

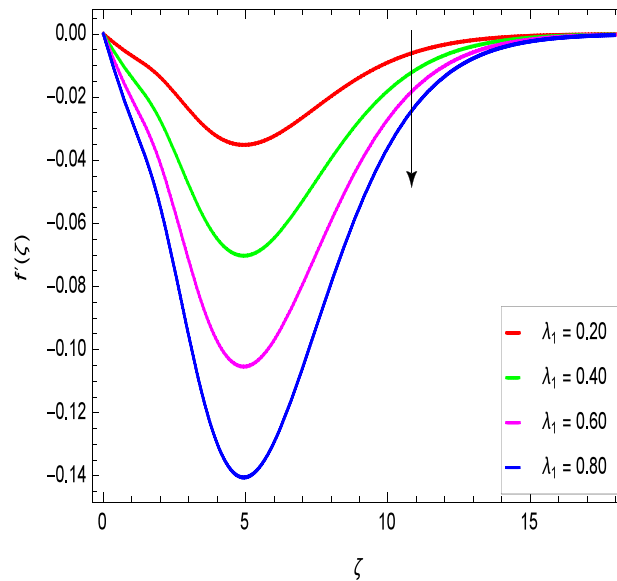


**Figure 2.**  $f'(\zeta)$  in terms of  $\lambda_1$ .

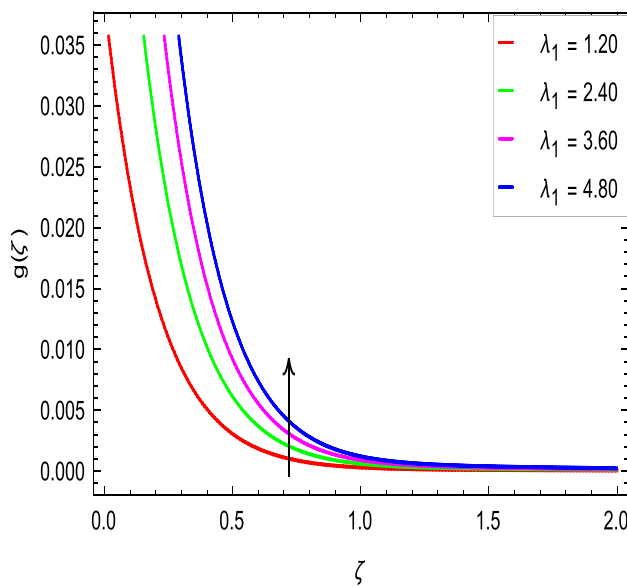


**Figure 3.**  $g(\zeta)$  in terms of  $\lambda_1$ .

**Velocity profiles.** Figures 2 and 3 show the impact of the rotation parameter on the velocity profiles. For elevating values of the rotation parameter  $\lambda_1$ , the velocity  $f'$  is weakened and the velocity  $g$  is enhanced by higher values of rotation parameter  $\lambda_1$ . The physical interpretation for this feature is attributed to the reduction of momentum and thermal boundary layers, which lead to an increase in the gradients of nanofluid velocity. Figure 4 shows a declining trend in velocity  $f'$  for the higher estimation of the ferromagnetic parameter  $\beta$ . Physically higher values develop more resistance to fluid flow. At the end, it reduces the velocity profile. Figure 5 shows a growing trend in velocity  $f'$  for the larger values of  $\gamma_1$ . This can be perceived as buoyancy aspects understanding, the convection cooling effects are enhanced by a strong acceleration of the flow. Figure 6 shows that the dimensionless velocity decreases with an increase in the buoyancy ratio parameter  $Nr$  leading to an increase in the negative buoyant force caused by the presence of nanoparticles. The effect of increasing the bioconvection Rayleigh number  $Rb$  is that the convection power caused by bioconvection is enhanced against the convection of the buoyancy force. As a result, it could be noted that the flow velocity decreases with increasing the bioconvection Rayleigh number  $Rb$  values as shown in Fig. 7. Figure 8 is plotted here to measure the velocity variance against the viscoelastic parameter  $A_1$ . The increasing velocity trend is aligned with the rising viscoelastic parameter  $A_1$ . This behavior is rationalized by the mathematical representation of  $A_1 = \alpha_1 c_1 / \mu_{f_\infty}$  that, by increasing



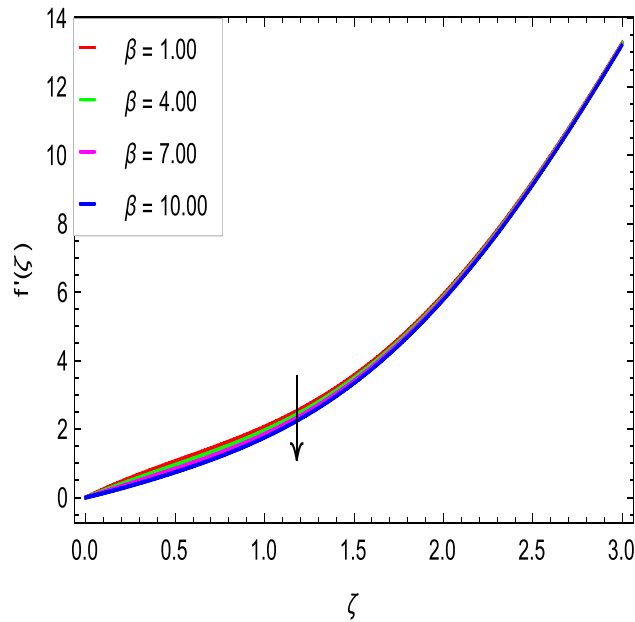


**Figure 4.**  $f'(\zeta)$  in terms of  $\beta$ .

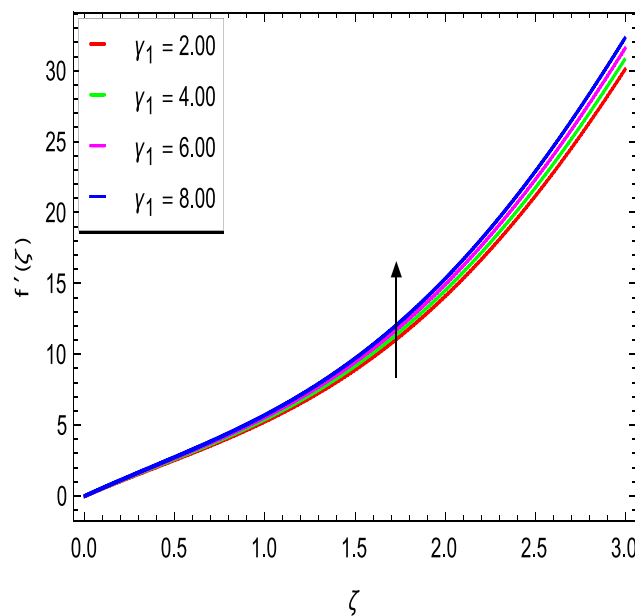


**Figure 5.**  $f'(\zeta)$  in terms of  $\gamma_1$ .

the magnitude of  $A_1$ , the viscosity decreases due to the velocity of the fluid. Mounts and the chaotic behavior of the uplifters are seen. It is efficient to note that the present problem reduces to the Newtonian case when  $A_1 = 0$ . From the boundary layer point of view, the thickness of the fluid increases with an increase in the viscoelastic parameter  $A_1$ . The opposite trend of velocity  $g$  for the viscoelastic parameter  $A_1$  is observed as shown in Fig. 9.

**Temperature profile.** Figure 10 is used to measure the effect of the ferromagnetic parameter  $\beta$  on temperature. The temperature here rises with the greater values of ferromagnetic parameter  $\beta$ . The effect of the heat dissipation parameter  $\lambda$  on temperature is shown in Fig. 11. The temperature here increases with an increase in the the heat dissipation parameter  $\lambda$ . Physically thermal conductivity of the fluid decays with the higher values of heat dissipation parameter  $\lambda$ . The temperature characteristics with the curie temperature parameter  $\varepsilon$  are shown in Fig. 12. The temperature decreases in the estimation of the curie temperature parameter  $\varepsilon$ . Nanofluid thermal conductivity increases with the increase in the curie temperature  $\varepsilon$ . In effect, the added heat is removed and the temperature rises from the surface to the nanofluid. Figure 13 shows variations in temperature for the

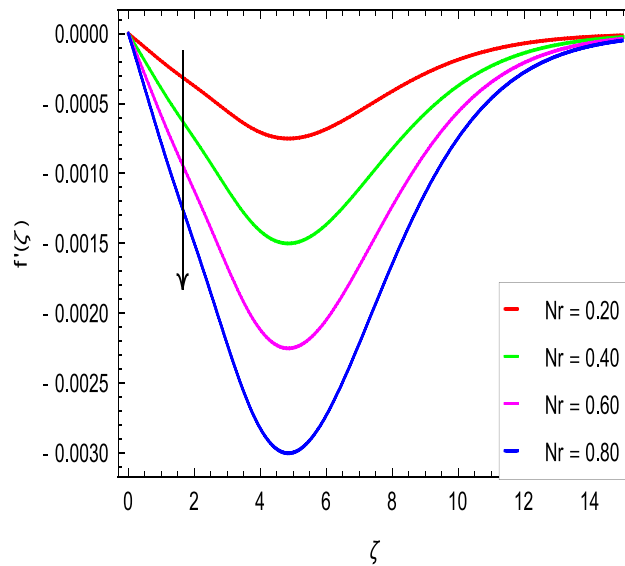


**Figure 6.**  $f'(\zeta)$  in terms of  $Nr$ .

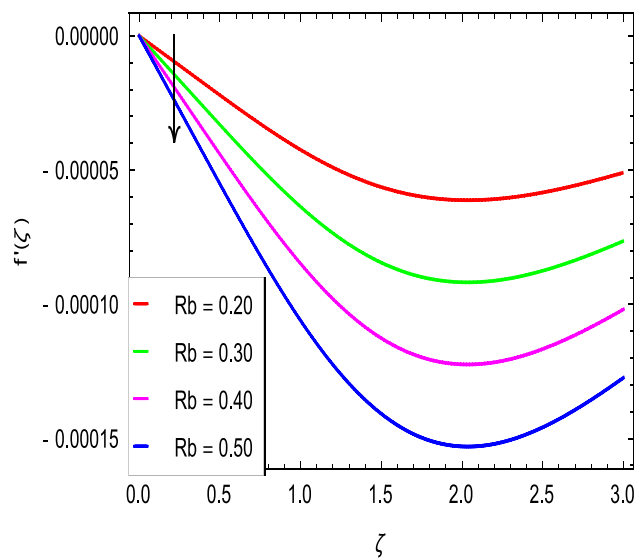


**Figure 7.**  $f'(\zeta)$  in terms of  $Rb$ .

increasing values of Prandtl number  $Pr$ . For the higher values of the Prandtl number  $Pr$ , the temperature of the nanofluid decreases. Figure 14 shows the response of the thermal Biot number  $Bi$  to the temperature profile. The temperature is indicated to rise as a result of the increase in the thermal Biot number values. Thermal Biot number  $Bi$  depends on the coefficient of heat transfer or is directly proportional to the coefficient of heat transfer. Figure 15 shows that the non-dimensional temperature and thermal boundary layer thickness decrease as the thermophoresis parameter  $Nt$  increases. The extra energy produced by the interaction of nanoparticles with the fluid due to the thermophoresis effect reduces the temperature. As a result, the thickness of the thermal boundary layer is reduced by higher values of the thermophoresis parameter  $Nt$ . As shown in Fig. 16, the dimensionless temperature and thermal boundary layer thickness are increased with an increase in Brownian motion parameter  $Nb$ . The additional heat generated by the interaction between nanoparticles and the fluid due to Brownian motion increases the temperature. As a result, the thermal boundary layer thickness enhances with the positive values of the Brownian motion parameter  $Nb$ .

**Nanoparticles concentration profile.** The Schmidt number  $Sc$  is attributed to mass diffusion and therefore increases the mass diffusivity leading to a lower concentration of nanoparticles due to less mass diffusion transport, as shown in Fig. 17. Figure 18 shows that the concentration of nanoparticles and hence the thickness of concentration boundary layer increase with the increase of the Brownian motion parameter  $Nb$ . Figure 19

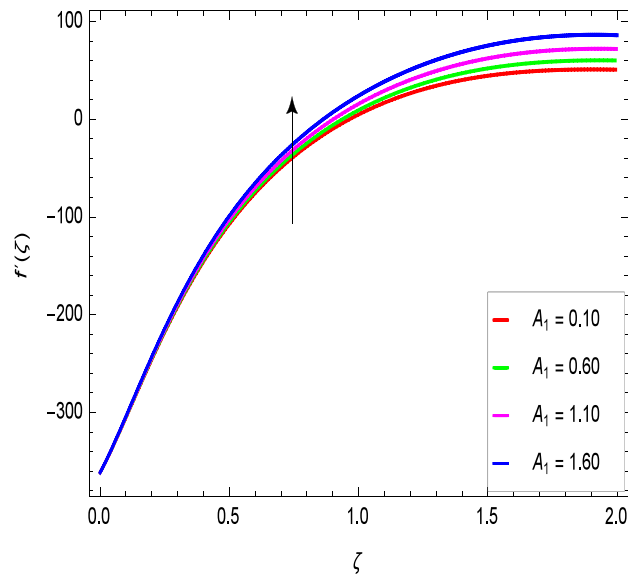


**Figure 8.**  $f'(\zeta)$  in terms of  $A_1$ .

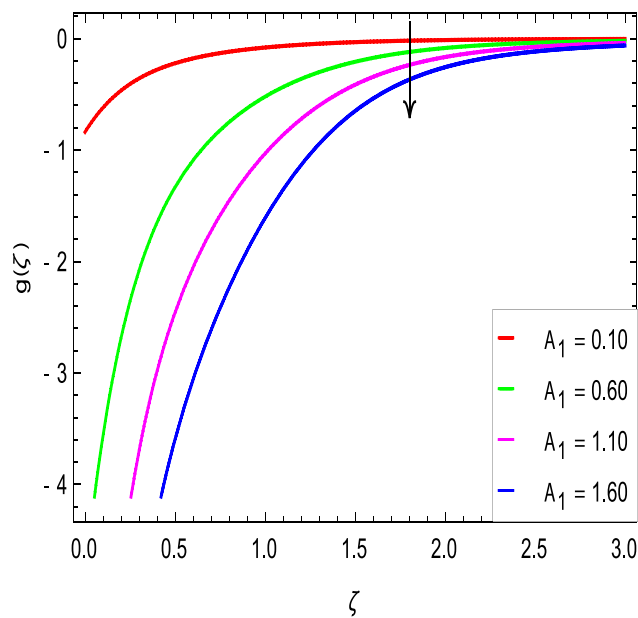


**Figure 9.**  $g(\zeta)$  in terms of  $A_1$ .

shows that the concentration of nanoparticles decreases as thermophoresis parameter  $Nt$  increases. Thus, it can be deduced that the boundary layer thickness of nanoparticles with the thermophoresis parameter  $Nt$  becomes less thick.

**Motile microorganisms concentration profile.** Figure 20 shows the effect of the rotation parameter  $\lambda_1$  on the motile microorganism density for the elevated values which increases the density of the motile microorganisms. Due to the strong relation of parameter in the governing equation 18 for the microorganisms, the dimensionless density of the motile microorganisms is highly influenced by the bioconvection Schmidt number  $Sb$ . It can be seen from Fig. 21 that the rising values of  $Sb$  reduces the dimensionless density of the motile microorganisms profile. This is due to the bioconvection Schmidt number  $Sb$  which aids in the weakening of microorganisms concentration layer thickness, as indicated. The effect of the bioconvection Rayleigh number  $Rb$  on the density of motile microorganisms fluctuations is shown in Fig. 22. It is clear that the bioconvection Rayleigh number  $Rb$  is enhancing the motile microorganisms. Of course, the Biot number  $Bi$  strengthens the convective

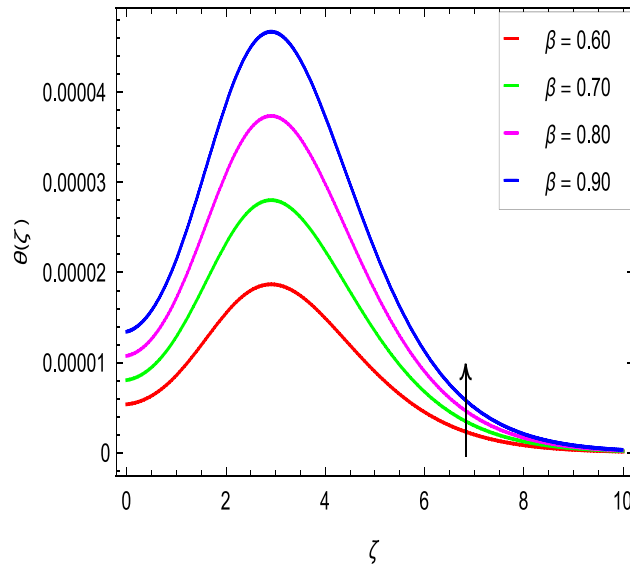


**Figure 10.**  $\theta(\zeta)$  in terms of  $\beta$ .

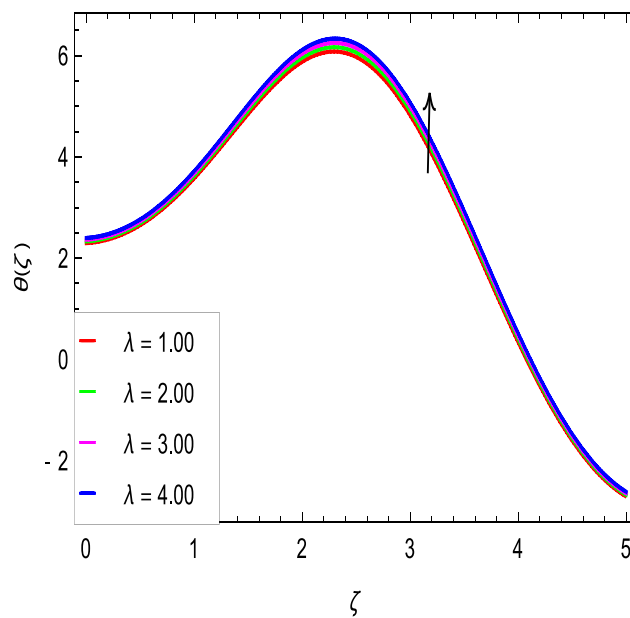


**Figure 11.**  $\theta(\zeta)$  in terms of  $\lambda$ .

heat transfer from the hot nanofluid domain to the cold nanofluid portion on the surface of the sphere. It is clear that the improvement in the Biot number  $Bi$  results in more improvement in convective heating and density of motile microorganisms increases as seen in Fig. 23. The effects of Peclet number  $Pe$  and the concentration difference parameter on the motile microorganisms profile are shown in Figs. 24 and 25 respectively. This would be related to the fact that the concentration of motile micro-organisms within the boundary layer decreases as these parameters increase.

### Conclusion

Analysis of the thermodynamics with the dipole effect and microorganisms shows that flow and heat transfer are enhanced with rotation parameter while for the magnetic dipole effect they have the opposite trend. Prandtl number has the cooling effect and the heat transfer increases with convective conditions. Nanoparticles concentration is improved with the Brownian motion parameter while the motile microorganisms motion is also enhanced with the rotation parameter, bioconvection Rayleigh number and convective condition.

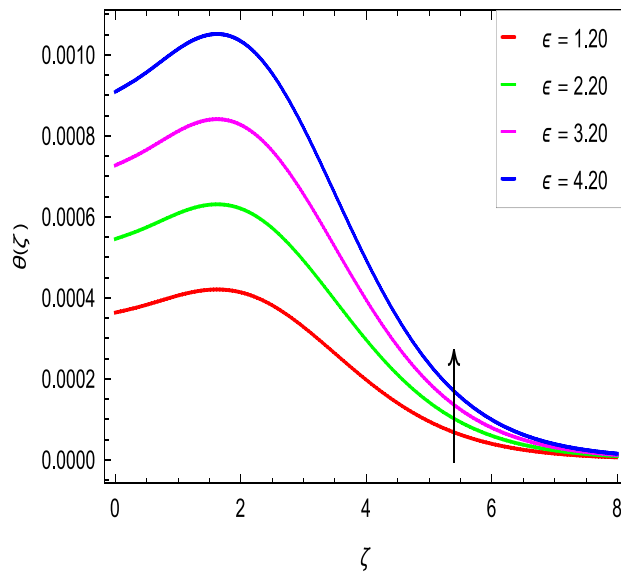


**Figure 12.**  $\theta(\zeta)$  in terms of  $\epsilon$ .

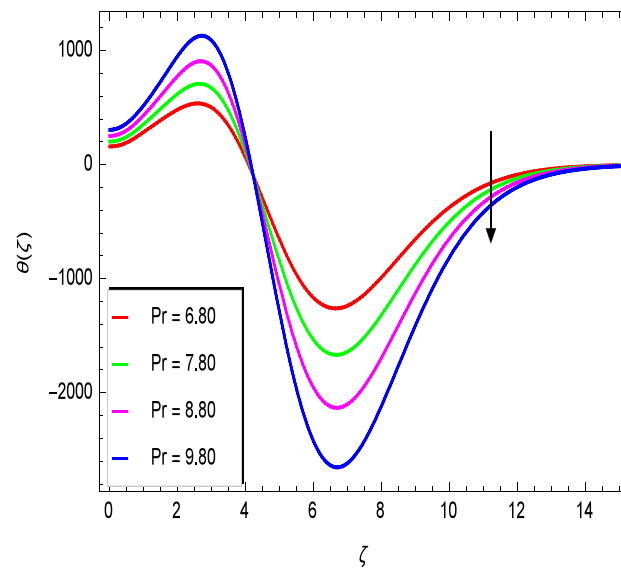


**Figure 13.**  $\theta(\zeta)$  in terms of  $Pr$ .

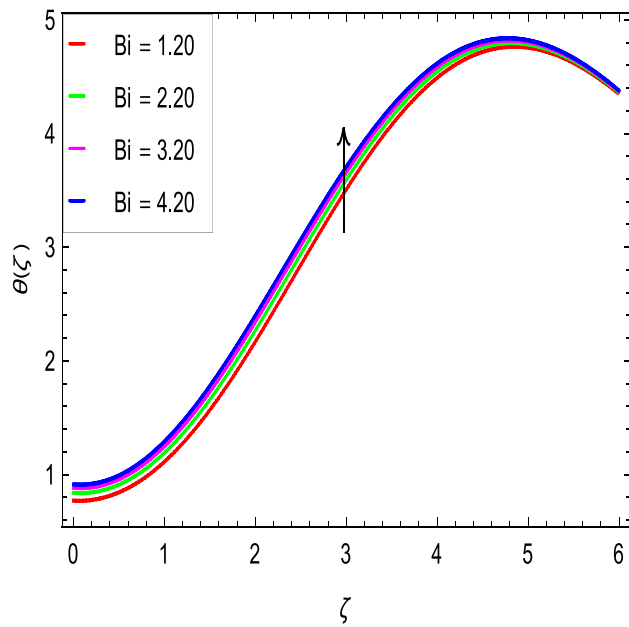


**Figure 14.**  $\theta(\zeta)$  in terms of  $Bi$ .

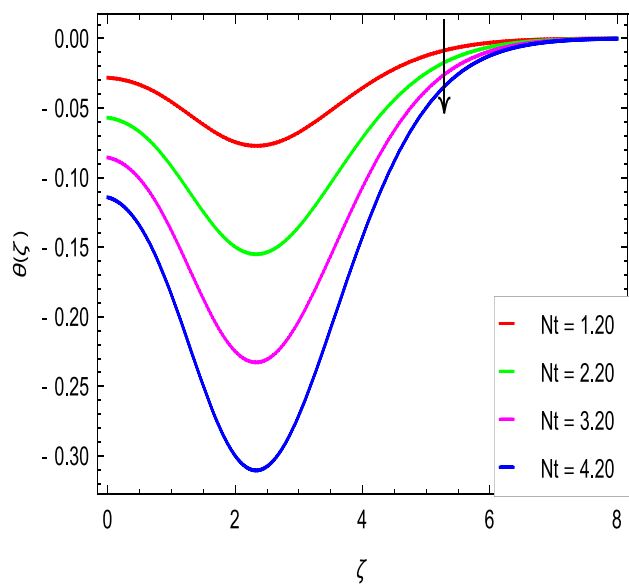


**Figure 15.**  $\theta(\zeta)$  in terms of  $Nt$ .

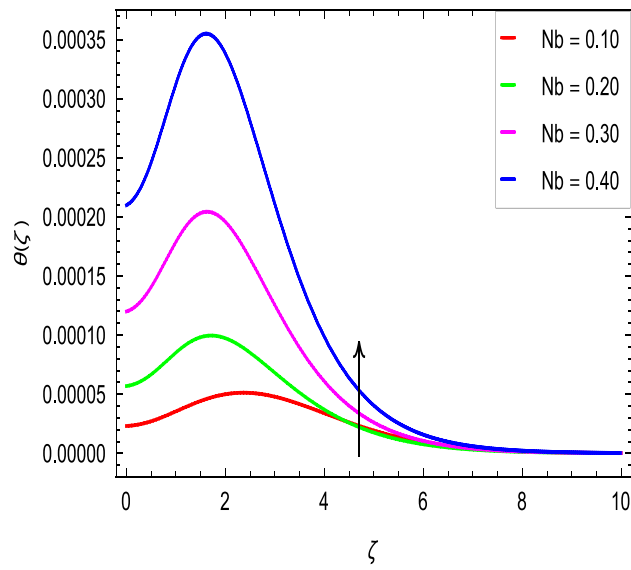


**Figure 16.**  $\theta(\zeta)$  in terms of  $Nb$ .

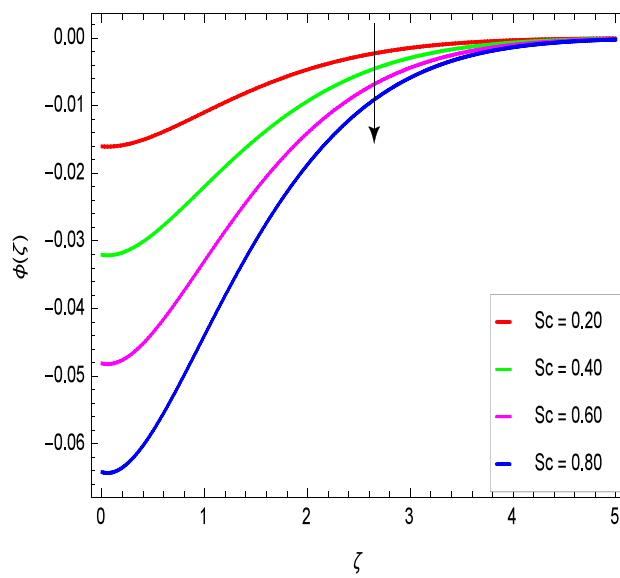


**Figure 17.**  $\phi(\zeta)$  in terms of  $Sc$ .

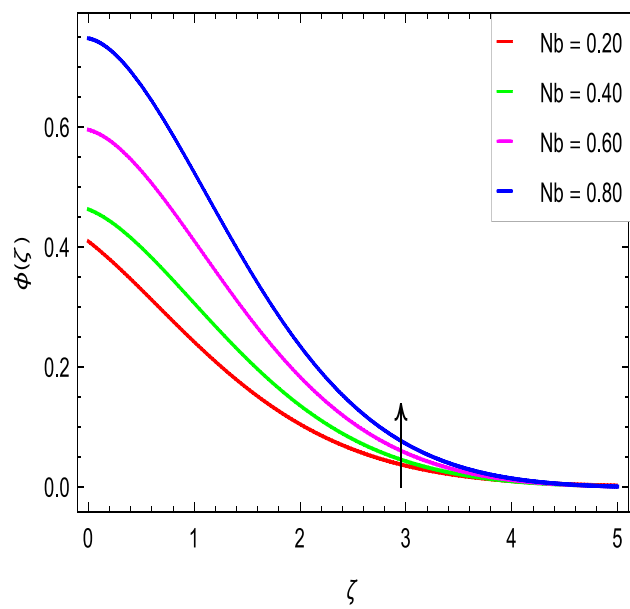


**Figure 18.**  $\phi(\zeta)$  in terms of  $Nb$ .

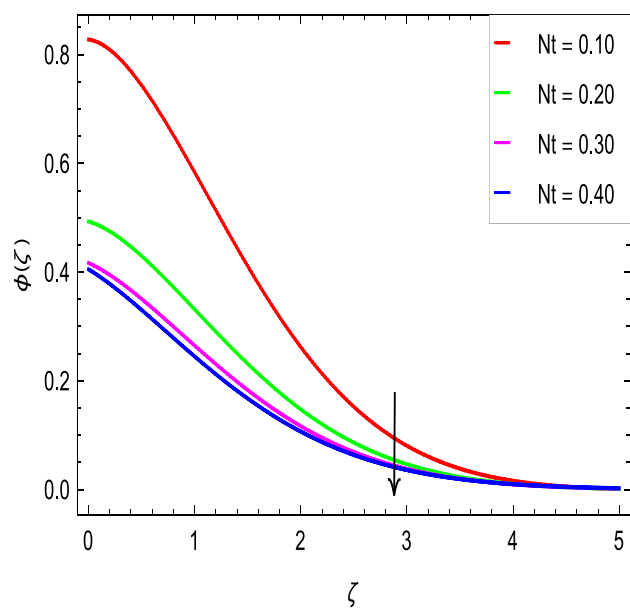


**Figure 19.**  $\phi(\zeta)$  in terms of  $Nt$ .



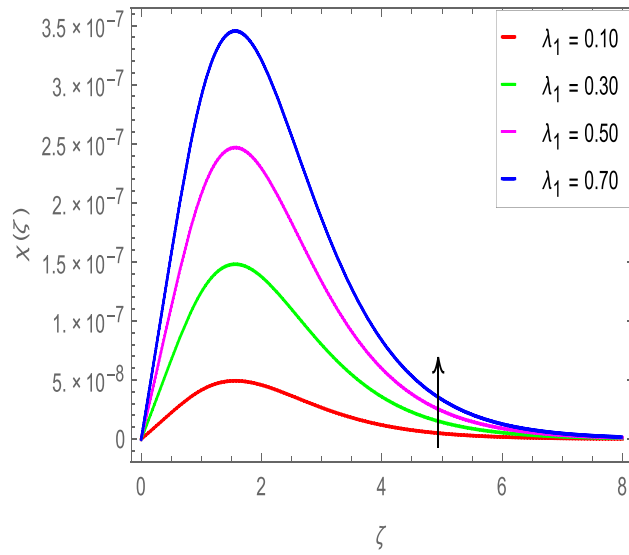


**Figure 20.**  $\chi(\zeta)$  in terms of  $\lambda_1$ .

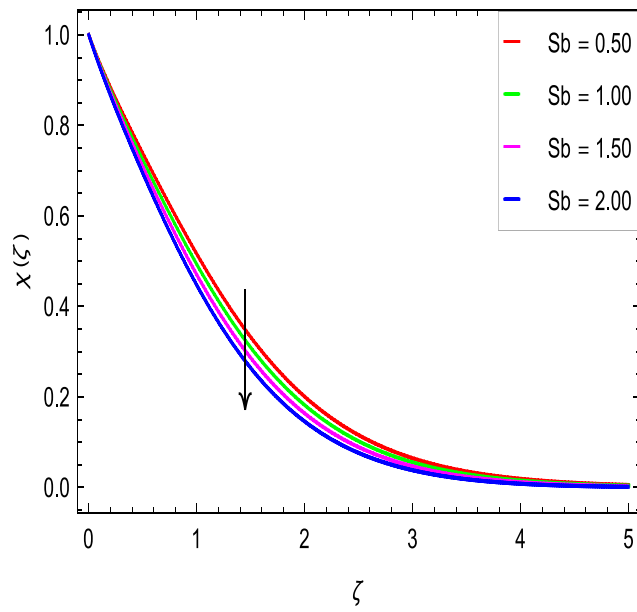


**Figure 21.**  $\phi(\zeta)$  in terms of  $Sb$ .

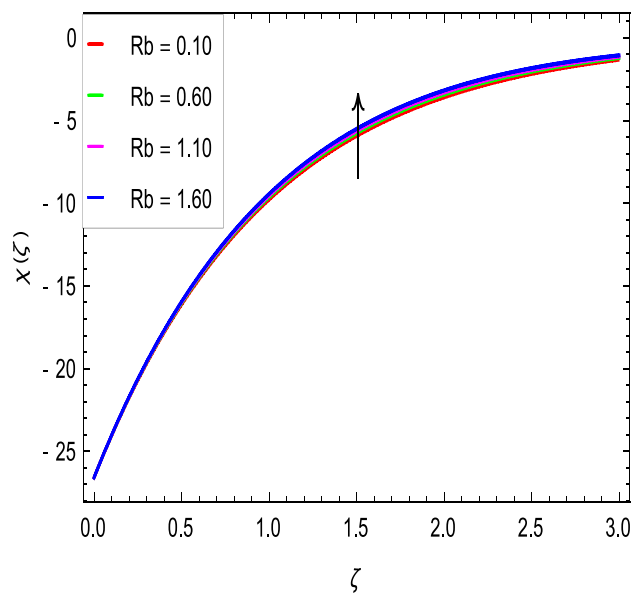


**Figure 22.**  $\chi(\zeta)$  in terms of  $Rb$ .

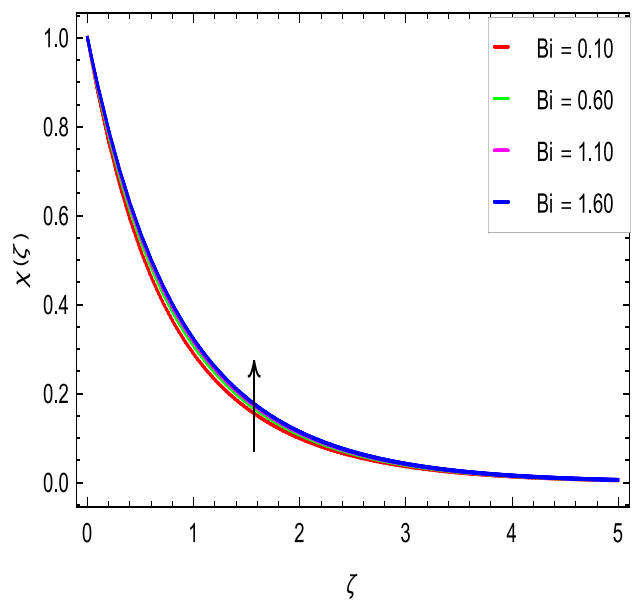


**Figure 23.**  $\chi(\zeta)$  in terms of  $Bi$ .

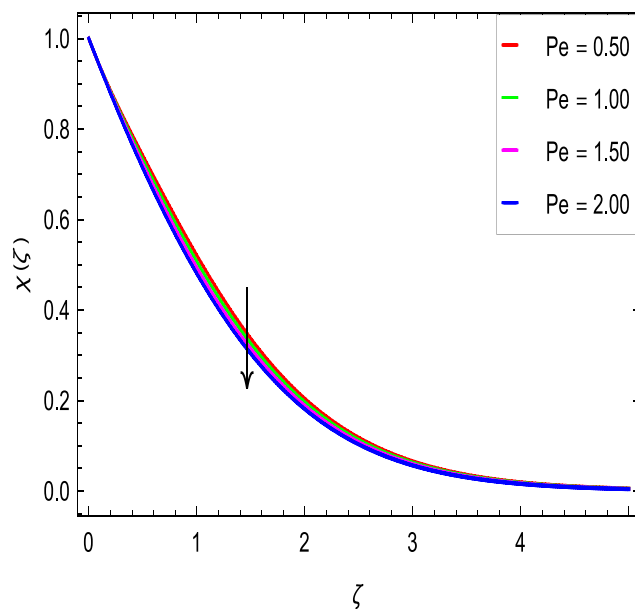


**Figure 24.**  $\chi(\zeta)$  in terms of  $Pe$ .

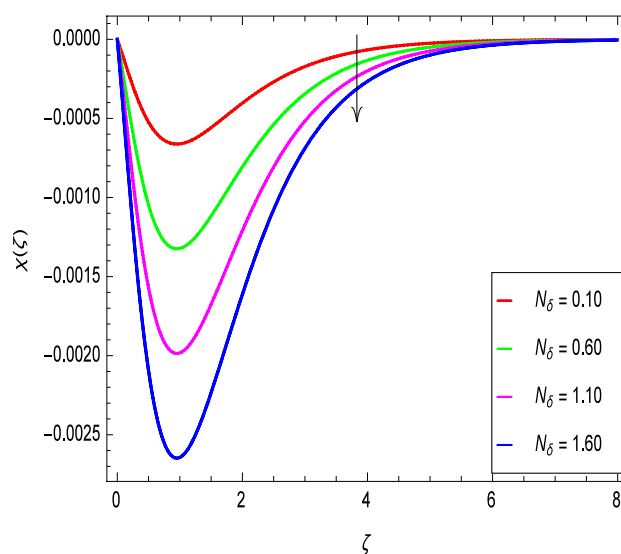


**Figure 25.**  $\chi(\zeta)$  in terms of  $N_\delta$ .

### Data availability

Availability exists for whole of the data.

Received: 18 February 2021; Accepted: 10 June 2021

Published online: 30 June 2021

### References

1. Raj, K. & Moskowitz, R. Commercial applications of ferrofluids. *J. Magn. Magn. Mater.* **85**, 233–245 (1990).
2. Zeeshan, A., Majeed, A. & Ellahi, R. Effect of magnetic dipole on viscous ferro-fluid past a stretching surface with thermal radiation. *J. Mol. Liq.* **215**, 549–554 (2016).
3. Hathway, D. B. dB-sound. *Eng. Mag.* **13**, 42–44 (1979).
4. Andersson, H. I. & Valnes, O. A. Flow of a heated ferrofluid over a stretching sheet in the presence of a magnetic dipole. *Acta Mech.* **128**, 39–47 (1998).
5. Zeeshan, A., Majeed, A., Ellahi, R. & Zia, Q. M. Z. Mixed convection flow and heat transfer in ferromagnetic fluid over a stretching sheet with partial slip effects. *Therm. Sci.* **22**, 2515–2526 (2018).

6. Hayat, T., Ahmad, S., Khan, M. I. & Alsaedi, A. Exploring magnetic dipole contribution on radiative flow of ferromagnetic Williamson fluid. *Results Phys.* **8**, 545–551 (2018).
7. Khan, N. S. *et al.* Hall current and thermophoresis effects on magnetohydrodynamic mixed convective heat and mass transfer thin film flow. *J. Phys. Commun.* **3**, 035009 (2019).
8. Khan, N. S., Gul, T., Islam, S. & Khan, W. Thermophoresis and thermal radiation with heat and mass transfer in a magnetohydrodynamic thin film second-grade fluid of variable properties past a stretching sheet. *Eur. Phys. J. Plus* **132**, 11 (2017).
9. Khan, N. S. *et al.* Influence of inclined magnetic field on Carreau nanoliquid thin film flow and heat transfer with graphene nanoparticles. *Energies* **12**, 1459 (2019).
10. Khan, N. S. Study of two dimensional boundary layer flow of a thin film second grade fluid with variable thermo-physical properties in three dimensions space. *Filomat* **33**(16), 5387–5405 (2019).
11. Khan, N. S. & Zuhra, S. Boundary layer unsteady flow and heat transfer in a second grade thin film nanoliquid embedded with graphene nanoparticles past a stretching sheet. *Adv. Mech. Eng.* **11**(11), 1–11 (2019).
12. Khan, N. S., Gul, T., Islam, S., Khan, A. & Shah, Z. Brownian motion and thermophoresis effects on MHD mixed convective thin film second-grade nanofluid flow with Hall effect and heat transfer past a stretching sheet. *J. Nanofluids* **6**(5), 812–829 (2017).
13. Khan, N. S. *et al.* Lorentz forces effects on the interactions of nanoparticles in emerging mechanisms with innovative approach. *Symmetry* **12**(10), 1700 (2020).
14. Khan, N. S., Kumam, P. & Thounthong, P. Magnetic field promoted irreversible process of water based nanocomposites with heat and mass transfer flow. *Sci. Rep.* **1**, 11692 (2021).
15. Khan, N. S. *et al.* Magnetohydrodynamic nanoliquid thin film sprayed on a stretching cylinder with heat transfer. *Appl. Sci.* **7**, 271 (2017).
16. Khan, N. S., Kumam, P. & Thounthong, P. Second law analysis with effects of Arrhenius activation energy and binary chemical reaction on nanofluid flow. *Sci. Rep.* **10**, 1226 (2020).
17. Khan, N. S. *et al.* Slip flow of Eyring–Powell nanoliquid film containing graphene nanoparticles. *A.I.P. Adv.* **8**, 115302 (2019).
18. Ece, M. C. The initial boundary-layer flow past a translating and spinning rotational symmetric body. *J. Eng. Math.* **26**, 415–428 (1992).
19. Ece, M. C. & Öztürk, A. *Unsteady Forced Convection Heat Transfer at the Separation Point on a Spinning Sphere* No. CONF-950828-(ASME, 1995).
20. Takhar, H. S. & Girishwar, N. Self-similar solution of the unsteady flow in the stagnation point region of a rotating sphere with a magnetic field. *Heat Mass Transf.* **36**, 89–96 (2000).
21. Takhar, H. S., Chamkha, A. J. & Girishwar, N. Unsteady laminar MHD flow and heat transfer in the stagnation region of an impulsively spinning and translating sphere in the presence of buoyancy forces. *Heat Mass Transf.* **37**, 397–402 (2001).
22. Chamkha, A. J., Takhar, H. S. & Girishwar, N. Unsteady MHD rotating flow over a rotating sphere near the equator. *Acta Mech.* **164**, 31–46 (2003).
23. Anilkumar, D. & Roy, S. Self-similar solution of the unsteady mixed convection flow in the stagnation point region of a rotating sphere. *Heat Mass Transf.* **40**, 487–493 (2004).
24. Sweet, E., Kuppapalalle, V. & Robert, G. Analytical solutions for the unsteady MHD rotating flow over a rotating sphere near the equator. *Open Phys.* **9**, 167–175 (2011).
25. Turkyilmazoglu, M. Bödewad flow and heat transfer over a stretching stationary disk. *Int. J. Mech. Sci.* **90**, 246–250 (2015).
26. Bég, O. A., Mabood, F. & Islam, M. N. Homotopy simulation of nonlinear unsteady rotating nanofluid flow from a spinning body. *Int. J. Eng. Math.* **2015**, 1–15 (2015).
27. Calabretto, S. A. W., Levy, J. P. D. B. & Trent, W. M. The unsteady flow due to an impulsively rotated sphere. *Proc. Roy. Soc. A: Math. Phys. Eng. Sci.* **471**, 20150299 (2015).
28. Usman, A. H. *et al.* Development of dynamic model and analytical analysis for the diffusion of different species in non-Newtonian nanofluid swirling flow. *Front. Phys.* **8**, 616790 (2021).
29. Mahdy, A. Simultaneous impacts of MHD and variable wall temperature on transient mixed Casson nanofluid flow in the stagnation point of rotating sphere. *Appl. Math. Mech.* **39**, 1327–1340 (2018).
30. Mahdy, A. & Hossam, A. N. Microorganisms time-mixed convection nanofluid flow by the stagnation domain of an impulsively rotating sphere due to Newtonian heating. *Results Phys.* **19**, 103347 (2020).
31. Khan, N. S., Kumam, P. & Thounthong, P. Computational approach to dynamic systems through similarity measure and homotopy analysis method for the renewable energy. *Crystals* **10**(12), 1086 (2020).
32. Khan, N. S., Shah, Z., Shutaywi, M., Kumam, P. & Thounthong, P. A comprehensive study to the assessment of Arrhenius activation energy and binary chemical reaction in swirling flow. *Sci. Rep.* **10**, 7868 (2020).
33. Khan, N. S. *et al.* Rotating flow assessment of magnetized mixture fluid suspended with hybrid nanoparticles and chemical reactions of species. *Sci. Rep.* **11**(1), 11277 (2021).
34. Ibrahim, M. Numerical analysis of time-dependent flow of viscous fluid due to a stretchable rotating disk with heat and mass transfer. *Result Phys.* **18**, 103242 (2020).
35. Ibrahim, M., Saeed, T., Alshehri, A. M. & Chu, Y. M. The numerical simulation and sensitivity analysis of a non-Newtonian fluid flow inside a square chamber exposed to a magnetic field using the FDLBM approach. *J. Therm. Anal. Calorim.* **144**, 1–19 (2021).
36. Khan, N. S. *et al.* Entropy generation in MHD mixed convection non-Newtonian second grade nanoliquid thin film flow through a porous medium with chemical reaction and stratification. *Entropy* **21**, 139 (2021).
37. Khan, N. S., Zuhra, S. & Shah, Q. Entropy generation in two phase model for simulating flow and heat transfer of carbon nanotubes between rotating stretchable disks with cubic autocatalysis chemical reaction. *Appl. Nanosci.* **9**, 1797–822 (2019).
38. Khan, N. S., Gul, T., Khan, M. A., Bonyah, E. & Islam, S. Mixed convection in gravity-driven thin film non-Newtonian nanofluids flow with gyrotactic microorganisms. *Results Phys.* **7**, 4033–4049 (2017).
39. Amaratunga, M., Rabenjafimanantsoa, H. A. & Time, R. W. Estimation of shear rate change in vertically oscillating non-Newtonian fluids: Predictions on particle settling. *J. Non-Newton. Fluid* **277**, 104236 (2020).
40. Khan, N. S., Kumam, P. & Thounthong, P. Renewable energy technology for the sustainable development of thermal system with entropy measures. *Int. J. Heat Mass Transf.* **145**, 118713 (2019).
41. Khan, N. S., Shah, Q. & Sohail, A. Dynamics with Cattaneo–Christov heat and mass flux theory of bioconvection Oldroyd-B nanofluid. *Adv. Mech. Eng.* **12**(7), 1–20 (2020).
42. Hayat, T., Naveed, A., Sajid, M. & Saleem, A. On the MHD flow of a second-grade fluid in a porous channel. *Comput. Math. Appl.* **54**, 407–414 (2007).
43. Khan, M. & Masood, U. R. Flow and heat transfer to modified second grade fluid over a non-linear stretching sheet. *AIP Adv.* **5**, 087157 (2015).
44. Salahuddin, T., Arif, A., Haider, A. & Malik, M. Y. Variable fluid properties of a second-grade fluid using two different temperature-dependent viscosity models. *J. Braz. Soc. Mech. Sci. Eng.* **40**, 1–9 (2018).
45. Bilal, S. *et al.* Heat and mass transfer in hydromagnetic second-grade fluid past a porous inclined cylinder under the effects of thermal dissipation, diffusion and radiative heat flux. *Energies* **13**, 278 (2020).
46. Choi, S. U. & Eastman, J. A. *Enhancing Thermal Conductivity of Fluids with Nanoparticles* (Argonne National Lab, 1995).
47. El-Shorbagy, M. A. *et al.* Numerical investigation of mixed convection of nanofluid flow in a trapezoidal channel with different aspect ratios in the presence of porous medium. *Case Stud. Therm. Eng.* **25**, 100977 (2021).

48. Ali, V. *et al.* Navigating the effect of tungsten oxide nano-powder on ethylene glycol surface tension by artificial neural network and response surface methodology. *Powder Technol.* **386**, 483–490 (2021).
49. Chu, Y. M. *et al.* Examining rheological behavior of MWCNT-TiO<sub>2</sub>/5W40 hybrid nanofluid based on experiments and RSM/ANN modeling. *J. Mol. Liq.* **333**, 115969 (2021).
50. Ibrahim, M. *et al.* Two-phase analysis of heat transfer and entropy generation of water-based magnetite nanofluid flow in a circular microtube with twisted porous blocks under a uniform magnetic field. *Powder Technol.* **384**, 522–541 (2021).
51. Ibrahim, M., Algehyne, E. A., Saeed, T., Berrouk, A. S. & Chu, Y. M. Study of capabilities of the ANN and RSM models to predict the thermal conductivity of nanofluids containing SiO<sub>2</sub> nanoparticles. *J. Therm. Anal. Calorim.* **12**, 1–11 (2021).
52. Ibrahim, M., Saeed, T., Algehyne, E. A., Khan, M. & Chu, Y. M. The effects of L-shaped heat source in a quarter-tube enclosure filled with MHD nanofluid on heat transfer and irreversibilities, using LBM: numerical data, optimization using neural network algorithm (ANN). *J. Therm. Anal. Calorim.* **144**, 1–14 (2021).
53. Kuznetsov, A. V. Nanofluid bio-thermal convection: simultaneous effects of gyrotactic and oxytactic micro-organisms. *Fluid Dyn. Res.* **43**, 055505 (2011).
54. Awais, M. *et al.* MHD effects on ciliary-induced peristaltic flow coatings with rheological hybrid nanofluid. *Coatings* **10**, 186 (2020).
55. Ellahi, R., Zeeshan, A., Hussain, F. & Abbas, T. Thermally charged MHD bi-phase flow coatings with non-Newtonian nanofluid and hafnium particles along slippery walls. *Coatings* **9**, 300 (2019).
56. Akermi, M. *et al.* Synthesis and characterization of a novel hydride polymer P-DSBT/ZnO nanocomposite for optoelectronic applications. *J. Mol. Liq.* **287**, 110963 (2019).
57. Kahshan, M., Lu, D. & Rahimi-Gorji, M. Hydrodynamical study of flow in a permeable channel: application to flat plate dialyzer. *Int. J. Hydrog. Energy* **44**, 17041–17047 (2019).
58. Chamkha, A. J., Rashad, A. M., Kameswaran, P. K. & Abdou, M. M. Radiation effects on natural bioconvection flow of a nanofluid containing gyrotactic microorganisms past a vertical plate with streamwise temperature variation. *J. Nanofluids* **6**, 587–595 (2017).
59. Rashad, A. M., Chamkha, A. J., Mallikarjuna, B. & Abdou, M. M. Mixed bioconvection flow of a nanofluid containing gyrotactic microorganisms past a vertical slender cylinder. *Front. Heat Mass Trans.* **10**, 21 (2018).
60. Sudhagar, P., Kameswaran, P. K. & Kumar, B. R. Gyrotactic microorganism effects on mixed convective nanofluid flow past a vertical cylinder. *J. Therm. Sci. Eng. Appl.* **11**, 6 (2019).
61. Raju, C. S. & Sandeep, N. Dual solutions for unsteady heat and mass transfer in bio-convection flow towards a rotating cone/plate in a rotating fluid. *Int. J. Eng. Res. Afr.* **20**, 161–176 (2016).
62. Hady, F. M., Mahdy, A., Mohamed, R. A. & Zaid, O. A. A. Effects of viscous dissipation on unsteady MHD thermo bioconvection boundary layer flow of a nanofluid containing gyrotactic microorganisms along a stretching sheet. *World J. Mech.* **6**, 505–526 (2016).
63. Hady, F. M., Mohamed, R. A., Mahdy, A. & Zaid, O. A. A. Non-Darcy natural convection boundary layer flow over a vertical cone in porous media saturated with a nanofluid containing gyrotactic microorganisms with a convective boundary condition. *J. Nanofluids* **5**, 765–773 (2016).
64. Zuhra, S., Khan, N. S. & Islam, S. Magnetohydrodynamic second grade nanofluid flow containing nanoparticles and gyrotactic microorganisms. *Comput. Math. Appl.* **37**, 6332–58 (2018).
65. Usman, A. H. *et al.* Computational optimization for the deposition of bioconvection thin Oldroyd-B nanofluid with entropy generation. *Sci. Rep.* **11**(1), 11641 (2021).
66. Khan, N. S. *et al.* A framework for the magnetic dipole effect on the thixotropic nanofluid flow past a continuous curved stretched surface. *Crystals* **11**(6), 645 (2021).
67. Liao, S. J. The Proposed Homotopy Analysis Method for the Solution of Nonlinear Problems. Ph.D. thesis, Shanghai Jiao Tong University (1992).
68. Liao, S. J. An explicit, totally analytic approximate solution for Blasius' viscous flow problems. *Int. J. Non-Linear Mech.* **34**(4), 759–778 (1999).
69. Liao, S. *Beyond Perturbation: Introduction to the Homotopy Analysis Method* (CRC Press, 2003).
70. Rashidi, M. M., Siddiqui, A. M. & Asadi, M. Application of homotopy analysis method to the unsteady squeezing flow of a second-grade fluid between circular plates. *Math. Probl. Eng.* **2010**, 706840 (2010).

## Acknowledgements

The authors wish to thank the editors and anonymous referees for their comments and suggestions. The authors acknowledge the financial support provided by the Center of Excellence in Theoretical and Computational Science (TaCS-CoE), KMUTT. Moreover, this research was supported by Chiang Mai University. This work was partially supported by the International Research Partnerships: Electrical Engineering Thai-French Research Center (EE-TFRC) between King Mongkut's University of Technology North Bangkok and Université de Lorraine under Grant KMUTNB-BasicR-64-17. The first author is thankful to the Higher Education Commission (HEC) Pakistan for providing the technical and financial support.

## Author contributions

N.S.K. and A.H.U. formulated, solved the problem and wrote the paper. A.K. and P.K. sketched the graphs. P.T. and U.W.H. performed the investigations.

## Competing interests

The authors declare no competing interests.

## Additional information

**Correspondence** and requests for materials should be addressed to N.S.K., A.K. or P.K.

**Reprints and permissions information** is available at [www.nature.com/reprints](http://www.nature.com/reprints).

**Publisher's note** Springer Nature remains neutral with regard to jurisdictional claims in published maps and institutional affiliations.



**Open Access** This article is licensed under a Creative Commons Attribution 4.0 International License, which permits use, sharing, adaptation, distribution and reproduction in any medium or format, as long as you give appropriate credit to the original author(s) and the source, provide a link to the Creative Commons licence, and indicate if changes were made. The images or other third party material in this article are included in the article's Creative Commons licence, unless indicated otherwise in a credit line to the material. If material is not included in the article's Creative Commons licence and your intended use is not permitted by statutory regulation or exceeds the permitted use, you will need to obtain permission directly from the copyright holder. To view a copy of this licence, visit <http://creativecommons.org/licenses/by/4.0/>.

© The Author(s) 2021